Electropolymerization Kinetics of a Binary Mixture of *o*-Phenylenediamine and 2-Aminobenzothiazole and Characterization of the Obtained Polymer Films

S. M. Sayyah,[1] S. S. Abd El-Rehim,[2] S. M. Kamal,[1] M. M. El-Deeb,[1] R. E. Azooz[1]

[1]*Polymer Research Laboratory, Department of Chemistry, Faculty of Science, Beni-Suef University, Beni-Suef 62514, Egypt*
[2]*Department of Chemistry, Faculty of Science, Ain Shams University, Cairo, Egypt*

Received 4 December 2008; accepted 28 March 2010
DOI 10.1002/app.32534
Published online 21 July 2010 in Wiley Online Library (wileyonlinelibrary.com).

ABSTRACT: Poly(*o*-phenylenediamine-co-2-aminobenzothiazole), P(*o*PD-co-2ABT), has been synthesized electrochemically from an aqueous acid medium. The initial rate of electrocopolymerization reaction on platinum electrode is small, and the rate law is Rate $= K_E [Na_2SO_4]^{0.48} [HCl]^{1.09} [M]^{2.08}$. The apparent activation energy (E_a) is found to be 57.44 kJ mol^{-1}. The polymer films obtained have been characterized by cyclic voltammetry, X-ray diffraction, elemental analysis, TGA, scanning electron microscopy, and IR-spectroscopy. The mechanism of the electrochemical polymerization reaction has been discussed. The monomer reactivity ratios (r_1 and r_2) were calculated using Fineman-Röss method. J Appl Polym Sci 119: 252–264, 2011

Key words: kinetics; electropolymerization; reactivity ratio; TGA; morphology

INTRODUCTION

The electropolymerization of aniline and its derivatives is of great interest.[1] Electropolymerization may occur anodically, where electron is donated from monomer to the anode (oxidation process) or cathodically by gaining electron from cathode (reduction process).

Ortho-phenylenediamine, *o*PD, and its polymer poly(*o*-phenylenediamine), P(*o*PD), have shown interesting properties and thus promising application in various aspects. P(*o*PD) can be obtained as a thin layer of self-limiting thickness on different conduction substrates via anodic electropolymerization processes.[1]

P(*o*PD) is a solid in its reduced form, the film is colorless and its oxidized form is red. Two interesting properties of P(*o*PD), different from those that are characteristic of usual conducting polymers like polyaniline makes it promising for applications in electrochemical and bioelectrochemical sensors[2]; As opposed to PAN, the conducting form of P(*o*PD) is its reduced state, whereas its oxidized state is insulating and P(*o*PD) film is permselective.

A thiazole (Th) unit is used as electron-acceptor unit to control the band gap of the π-conjugated polymers and oligomers through an alternating sequence of donor-acceptor units in the π-conjugated polymeric chains.

Benzothiazoles (BTs), a group of xenobiotic compounds containing a benzene ring fused with thiazole ring, have a wide spectrum of biological activity. BTs are used as fungicides in lumber and lethal production,[3] as antialgal agents,[4] and as slimicides in the paper and pulp industry.[5] Aminobenzothiazole (ABT) is an intermediate in dye production.

Ibrahim and Etaiw[6] studied the intercalation of Th and BTh derivatives undergo polymerization within the cavities of the 3D polymer. A new molecular composite having pronounced electric conductivity is formed.

Sayyah et al.[7] studied the electropolymerization and characterization of 2-amino-phenyl-thiazole on Pt-electrode in acid medium under different reaction conditions. They obtain an amorphous, homogeneous, and compact adhering film on Pt-electrode. Also, they studied[8] the electropolymerization and characterization of a binary mixture of 3-chloro aniline and 2-amino-phenyl-thiazole on Pt-electrode in acid medium under different reaction conditions. They obtain a block copolymer film on Pt-electrode.

The kinetic equation of the electropolymerization reactions of different substituted aromatic amines were calculated from existed microgravimetric data[9–14] from both the ex situ microgravimetric and electrochemical data[15] and from electrochemical data.[16]

In the present study, we intend to investigate the electropolymerization of a binary mixture of *o*-

Correspondence to: S. M. Sayyah (smsayyah@hotmail.com).

phenylenediamine (*o*PD) and 2-aminobenzothiazole (2ABT) on Pt electrode from aqueous HCl solution using cyclic voltammetry technique. The kinetics, optimum conditions, and mechanism of the electrochemical polymerization will be discussed using electrochemical data. Also, the copolymer structure will be given from Fineman-Röss calculations and characterization of the obtained copolymer film should be done by UV-visible, IR, elemental analysis, TGA, SEM, and X-ray diffraction.

EXPERIMENTAL

Materials

o-Phenylenediamine (Merck-Darmstadt, Germany) was purified by twice recrystallization from distilled water. Hydrochloric acid solution and dimethylformamide were provided by Riedel-de Haën, Germany and El-Nasser pharmaceutical Chemical Company (Cairo, Egypt), respectively. Anhydrous sodium sulfate and 2-aminobenzothiazole were provided by Merck (Darmstadt, Germany) and were used as received. All chemicals are analytical grade. All solutions were prepared under nitrogen atmosphere in freshly double-distilled water.

Cell and electrodes

A standard three-electrode cell was used in the cyclic voltammetry measurements with a saturated calomel electrode (SCE) as the standard reference electrode. The auxiliary electrode was a platinum wire. The dimensions of the platinum working electrode were 1 cm $\times$ 0.5 cm $\times$ 0.05 cm. Before each run, the working electrode was cleaned and washed with distilled water, rinsed with ethanol, and dried.

The electrochemical experiments were performed using the Potentiostat/Galvanostat Wenking PGS 95. The i-E curves were recorded by computer software from the same company (Model ECT).

IR, elemental analysis, UV-vis, and TGA

IR measurements were carried out using Shimadzu FTIR-340 Jasco spectrophotometer.

Elemental analysis was carried out in the microanalytical center at Cairo University by oxygen flask combustion and dosimat E415 titrator (Metrohm).

The ultraviolet-visible absorption spectra of the prepared polymer samples were measured using Shimadzu UV spectrophotometer (M160 PC) at room temperature in the range 200–900 nm using dimethylformamide as a solvent and reference.

TGA of the obtained polymer was performed using a Shimadzu DT-30 thermal analyzer (Shimadzu, Kyoto, Japan). The weight loss was measured from ambient temperature up to 600°C, at the rate of 20°C min^{-1} to determine the degradation rate of the polymer.

Scanning electron microscopy and X-ray diffraction

Scanning electron microscopic analysis was carried out using a JXA-840A Electron Probe Microanalyzer (JEOL, Tokyo, Japan). The X-ray diffractometer (Philips 1976 Model 1390, Netherlands) was operated under the following conditions that were kept constant for all the analysis processes:

X-ray tube: Cu; Scan speed: 8 degree min^{-1}; Current: 30 mA; Voltage: 40 kV; Preset time: 10 s.

RESULTS AND DISCUSSION

Electropolymerization of a binary mixture of *o*PD and 2ABT

Electropolymerization of the two separate monomers *o*-phenylenediamine (*o*PD), 2-aminobenzothiazole (2ABT) and the binary mixture of the two monomers with molar ratio 1 : 1 in deoxygenated aqueous acid medium in the presence of 0.5 *M* HCl and 0.1 *M* Na_2SO_4 at 303 K are represented in Figure 1(A–C), and the data are summarized in Table I. The data reveals that the anodic oxidation peaks: at 609 mV vs SCE in case of *o*PD, at 90 mV vs SCE in case of 2ABT, and at 532 mV vs SCE in mixture of *o*PD and 2ABT are attributed to the removal of electron from nitrogen atom of the amino group to form radical cation in all cases,[12] which react with another molecule of monomer to form dimmer radical cation and so on to form polymer or copolymer. Where, the second oxidation peak in case of 2ABT could be attributed to the conversion of polaron to bipolaron state.[12] The cathodic span of the reverse scan of the binary monomer mixture does not involve any cathodic peak.

Figure 2 shows the effect of repetitive cycling on the formation of the copolymer film from the deoxygenated aqueous solution containing 0.5 *M* HCl, 0.05 *M* comonomer (1 : 1) molar ratio, and 0.1 *M* Na_2SO_4 at 303 K. The data reveal that the peak current densities (i_p) decrease with the repetitive cycling. The decrease of the anodic currents could be attributed to the presence of a part of the polymer film on the electrode surface; therefore, the currents of the following anodic half cycle decrease. It is possible that the stability of the deposited film enhances with successive cycling, and therefore, the peak currents decrease with repetitive cycling. The potential position of the redox peak does not shift with increase of the number of cycles, indicating that the redox reaction is independent on the polymer thickness.

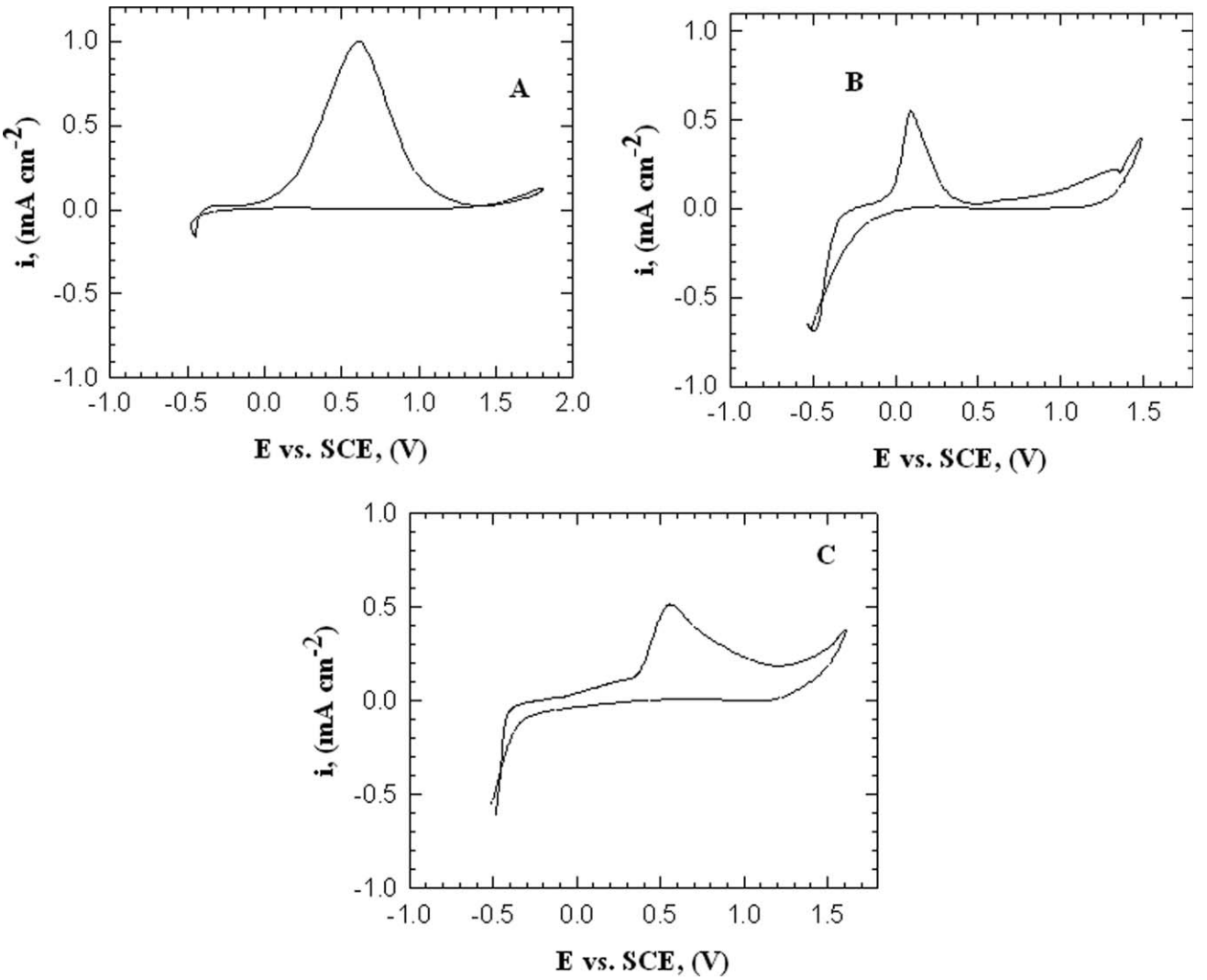

Figure 1 Cyclic voltammogram of Pt-electrode from deoxygenated solution containing 0.5 *M* HCl and 0.1 *M* Na_2SO_4 with scan rate of 25 mVs^{-1} in; A: 0.08 *M* *o*PD monomer, B: 0.001 *M* 2ABT monomer, and C: 0.05 *M* comonomer 1 : 1 molar ratio.

Figure 3(A) illustrates the influence of the scan rate (5–25 mVs^{-1}) on the potentiodynamic anodic polarization curves for the deoxygenated aqueous solution mixture containing 0.5 *M* HCl, 0.05 *M* monomer (1 : 1 molar ratio), and 0.1 *M* Na_2SO_4 at 303 K on platinum electrode. It is obvious that the anodic peak current densities (i_p) increases with the increasing of the scan rate. This behavior may be explained as follows, when an enough potential is

TABLE I
Cyclic Voltammetry Data for the Electropolymerization of P(*o*PD), P(2ABT), and P(*o*PD-co-2ABT) Samples

	Anodic oxidation peak potentials (mV vs SCE)	
Monomer name	1st peak	2nd peak
*o*PD	609	–
2ABT	90	1320
Comonomer mixture	532	–

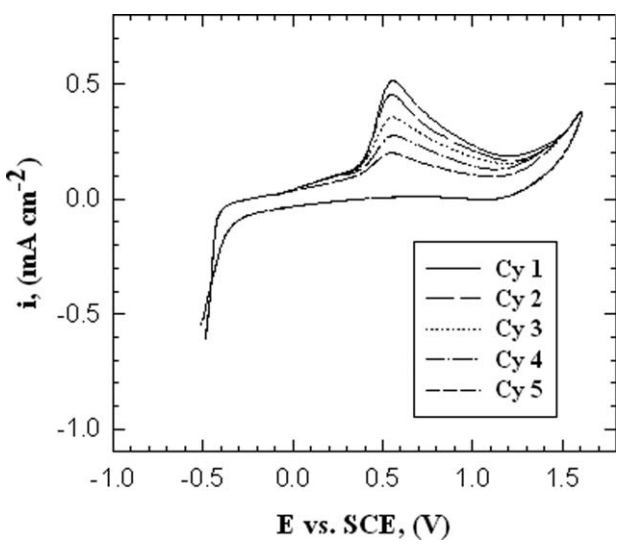

Figure 2 Effect of repetitive cycling on the formation of the copolymer film.

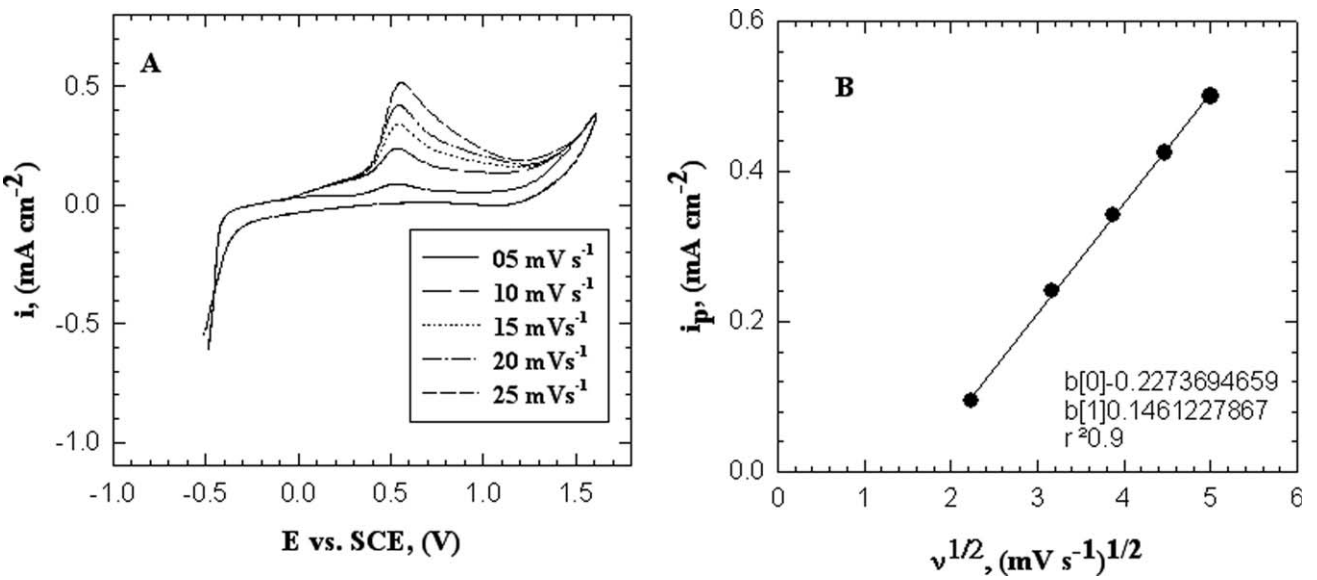

Figure 3 A: the influence of the scan rate (5–25 mVs^{-1}) on the potentiodynamic anodic polarization curves for mixture of *o*PD and 2ABT, B: the relation between i_p and $v^{1/2}$.

applied at an electrode surface causing oxidation of species in solution, a current arises due to the depletion of the species in the vicinity of the electrode surface. As a consequence, a concentration gradient appears in the solution. The current (i_p) is proportional to the gradient slope, dc/dx, imposed ($i\alpha \frac{dc}{dx}$). As the scan rate increase the gradient increase and consequently the current (i_p). Values of i_p is proportional directly to $v^{½}$ according to Randless[17] and Sevick[18] equation:

$$i_p = (2.69 \times 10^5) A n^{3/2} C D^{1/2} v^{1/2}$$

where A is constant, n is the number of exchanged electron in the mechanism, C is the bulk concentration, D is the diffusing coefficient, and v is the scan rate. The calculated D (0.5 M HCl, 0.05 M comonomer (1 : 1) molar ratio, 0.1 M Na_2SO_4, 303 K, and scan rate 25 mVs^{-1}) was found to be 7×10^{-6} m^2s^{-1}.

Figure 3(B) shows the linear dependence of the current peak, (i_p) versus $\nu^{1/2}$. This linear regression equation was

$$i_p(\text{mA}) = 0.146\ \nu^{1/2}(\text{mV s}^{-1})^{1/2} - 0.227$$

with a correlation coefficient of $r^2 = 0.999$. So we suggest that the electroformation of radical cation may be described partially by a diffusion-controlled process (diffusion of reacting species to the polymer film/solution interface).[19–21] It seems that, initially the electroformation of radical cation is controlled by charge transfer process. When the thickness of the polymer becomes thick, the diffusion of reactant inside the film becomes the slowest step, the process changed to diffusion transfer, which confirms the data in Figure 2.

The intercept in Figure 3(B) is small and negative, −0.227, which could be attributed to a decrease of the active area of the working electrode during the positive scan[22] or the increase of the covered area of working electrode by the adhered copolymer sample.

Kinetic studies

The electropolymerization kinetics were evaluated using deoxygenated aqueous solution containing monomer in the concentration range between 0.02 and 0.06 M, hydrochloric acid concentration in the range between 0.2 and 0.6 M, and Na_2SO_4 in the concentration range between (0.025 and 0.125 M) at 303 K.

From the values of the anodic current densities.[16,23] The electrochemical study of the copolymer formation is used instead of gravimetric study since the polymer yield on Pt-electrode is so small and the % conversion is few to be used in kinetic study.

The value of the anodic current density (i_p) is proportional to the electropolymerization rate ($R_{P,E}$) at a given concentration of the monomer, acid, and electrolyte, then we can replace the electropolymerization rate by the anodic current density.[16,23]

The influence of different experimental parameters affecting the electropolymerization reactions such as HCl concentration, monomer concentration, supporting electrolyte concentration, and temperature on platinum electrode surface was investigated.

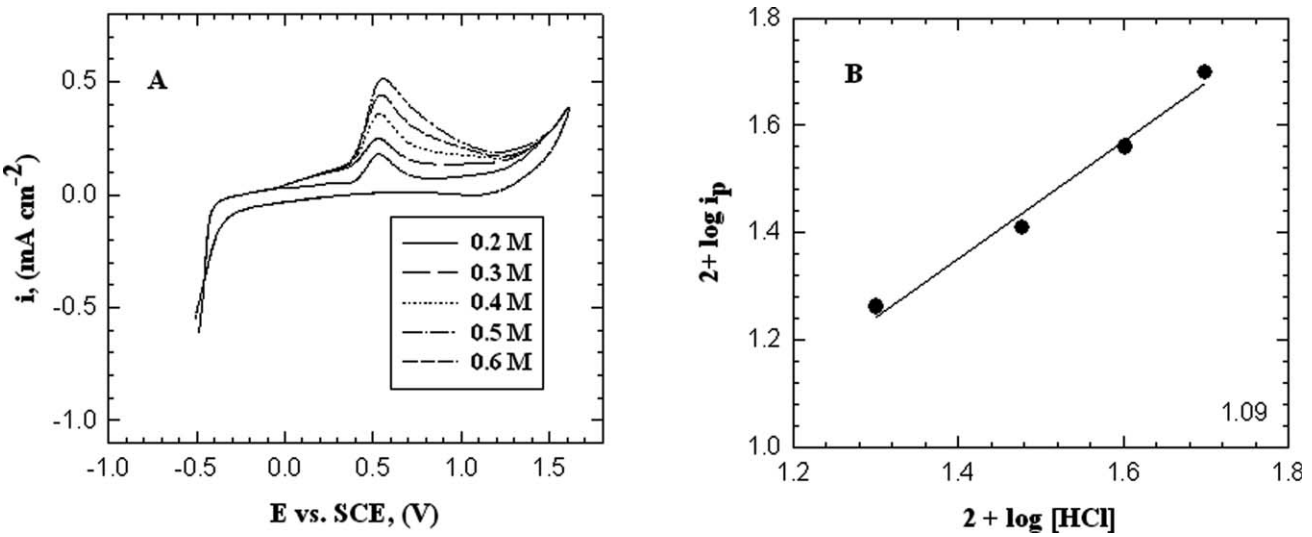

Figure 4 A: Cyclic voltammogram curves for the effect of HCl concentration on the electropolymerization of a binary mixture of *o*PD and 2ABT from solution containing 0.05 *M* (1 : 1 molar ratio) monomer and 0.1 *M* Na_2SO_4 at 303 K with scan rate of 25 mVs^{-1}. B: Double logarithmic plot of the anodic current densities versus HCl concentrations.

Effect of HCl concentration

Figure 4(A) represents the influence of HCl concentration in the range between (0.2 and 0.6 *M*) and 1 : 1 molar ratio on the cyclic voltammogram using scan rate of 25 mVs^{-1}. The voltammogram shows that the anodic peak current densities (i_p) and consequently the amount of copolymer increases with the increasing of the HCl concentration up to 0.5 *M* and then starts to decrease with further increase of HCl concentration. This could be attributed to the increase of the copolymer film conductivity with increase of the acid concentration, (i.e., acidity of the medium).[24] A double logarithmic plot of the current density related to oxidation peak against HCl concentrations in the range between 0.1 and 0.5 *M* is graphically represented in Figure 4(B). A straight line with a slope of 1.09 was obtained. Therefore, the reaction order with respect to the HCl concentration is a first-order reaction.

Effect of monomer concentration

Figure 5(A) represents the influence of the comonomer concentration in the range between (0.02 and 0.06 *M*) and 1 : 1 molar ratio on the cyclic voltammogram using scan rate of 25 mVs^{-1}. The voltammogram shows that the anodic peak current densities (i_p) increase with the increasing of the

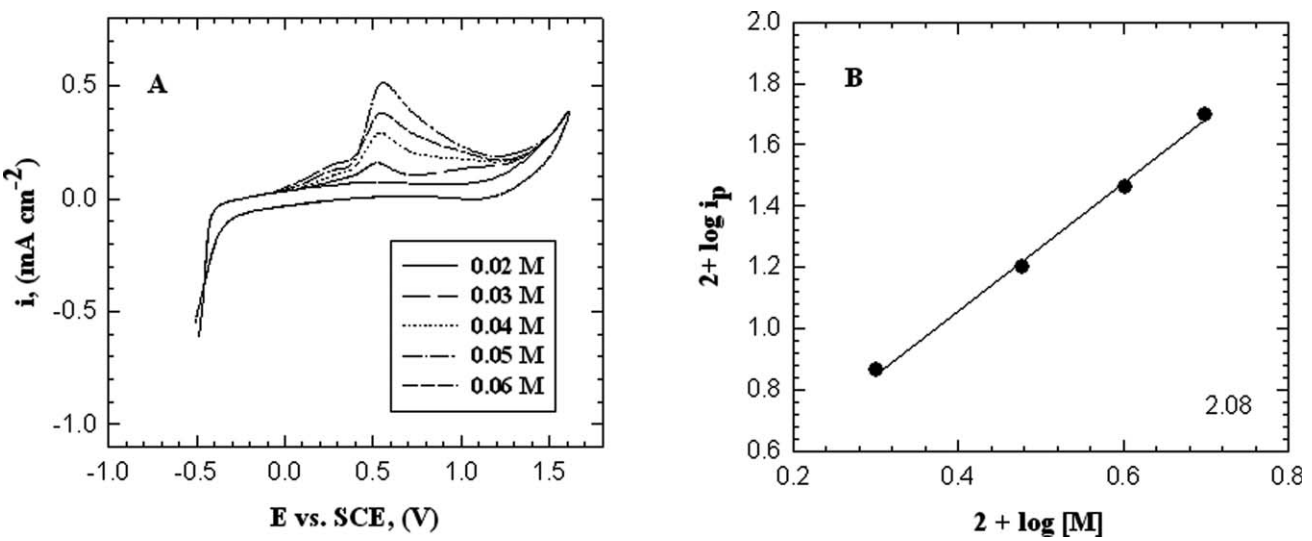

Figure 5 A: Cyclic voltammogram curves for the effect of monomer concentration on the electropolymerization of a binary mixture of *o*PD and 2ABT from solution containing 0.5 *M* HCl and 0.1 *M* Na_2SO_4 at 303 K with scan rate of 25 mVs^{-1}. B: Double logarithmic plot of the anodic current densities versus monomer concentrations.

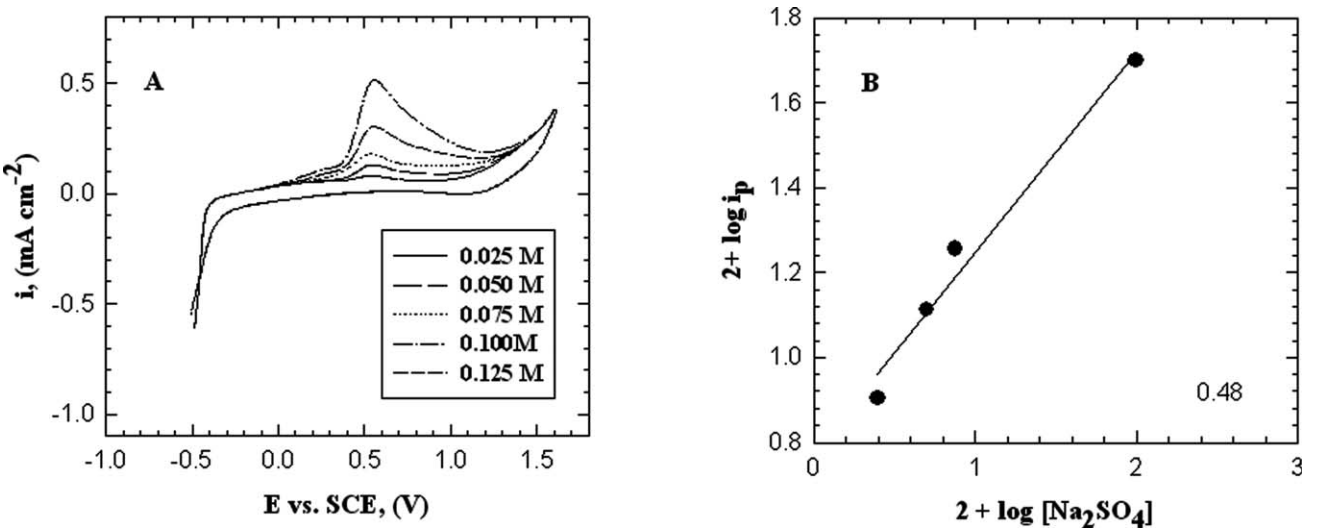

Figure 6 A: Cyclic voltammogram curves for the effect of Na_2SO_4 concentration on the electropolymerization of a binary mixture of *o*PD and 2ABT from solution containing 0.5 *M* HCl and 0.05 *M* (1 : 1 molar ratio) monomer at 303 K with scan of 25 mVs^{-1}. B: Double logarithmic plot of the anodic current densities versus Na_2SO_4 concentrations rate.

monomer concentration up to 0.05 *M* and then starts to decrease with further increase of the comonomer concentration. A double logarithmic plot of the current density values related to oxidation peak against monomer concentrations in the range between 0.01 and 0.05 *M* is graphically represented in Figure 5(B). A straight line with a slope of 2.08 was obtained. Therefore, the reaction order with respect to the monomer concentration is a second-order reaction.

Effect of electrolyte concentration

The effect of Na_2SO_4 concentration in the range between (0.025 and 0.125 *M*) on the cyclic voltammogram using scan rate of 25 mVs^{-1} is represented in Figure 6(A). The anodic peak current densities (i_p) increase with the increasing of the Na_2SO_4 concentration up to 0.1 *M* and then starts to decrease with further increase of Na_2SO_4 concentration. A double logarithmic plot of the current density values related to the oxidation peak against Na_2SO_4 concentrations in the range between 0.025 and 0.1 *M* is graphically represented in Figure 6(B). A straight line with slope of 0.48 was obtained. Therefore, the reaction order with respect to the electrolyte concentration is a half-order reaction.

Depending upon the above results, the kinetic rate law obtained from this method can be written as:

$$R_{P,E} = k_E[\text{monomer}]^{2.08}[\text{acid}]^{1.09}[\text{electrolyte}]^{0.48}$$

where, $R_{P,E}$ is the electropolymerization rate, k_E is the kinetic rate constant and [monomer] is the total concentration of monomers with composition (1 : 1) molar ratio.

Effect of temperature

The potentiodynamic polarization curves as a function of the solution temperature in the range between 288 and 313 K under the same experimental conditions as mentioned above are illustrated in Figure 7(A). From the figure, it is clear that an increase of the temperature up to 308 K results in a progressive increase of the current density value of the anodic peak. The plot of the log (i_p) versus $1/T$[25] is represented in Figure 7(B), a straight line is obtained with a slope equal to −3 and then the apparent activation energy was calculated using Arrhenius eq. [12] and it is found to be 57.44 kJ mol^{-1}.

The value of E_a at optimum conditions (0.1 *M* Na_2SO_4, 0.05 *M* comonomer (1 : 1 molar ratio), 0.5 *M* HCl and 308 K) is approximately the same at 20, 25, 30 mV s^{-1} as shown in Table II.

Elemental and spectroscopic analysis

Elemental analytical data are given in Table III, which are in a good agreement with those calculated from the suggested structure given in Scheme 1.

The presence of six water molecules for each repeated unit is confirmed by thermogravimetric analysis—the thermal degradation mechanism is complex and occurs in several steps (five steps). As shown in Figure 8 and Table IV:

- The first decomposition stage, between room temperature and 108°C starts with the loss of water. The weight loss for this stage was found to be 5.17 %, which is in good agreement with the calculated value (5.20 %). This is in a good agreement with literatures for water release.[12–16]

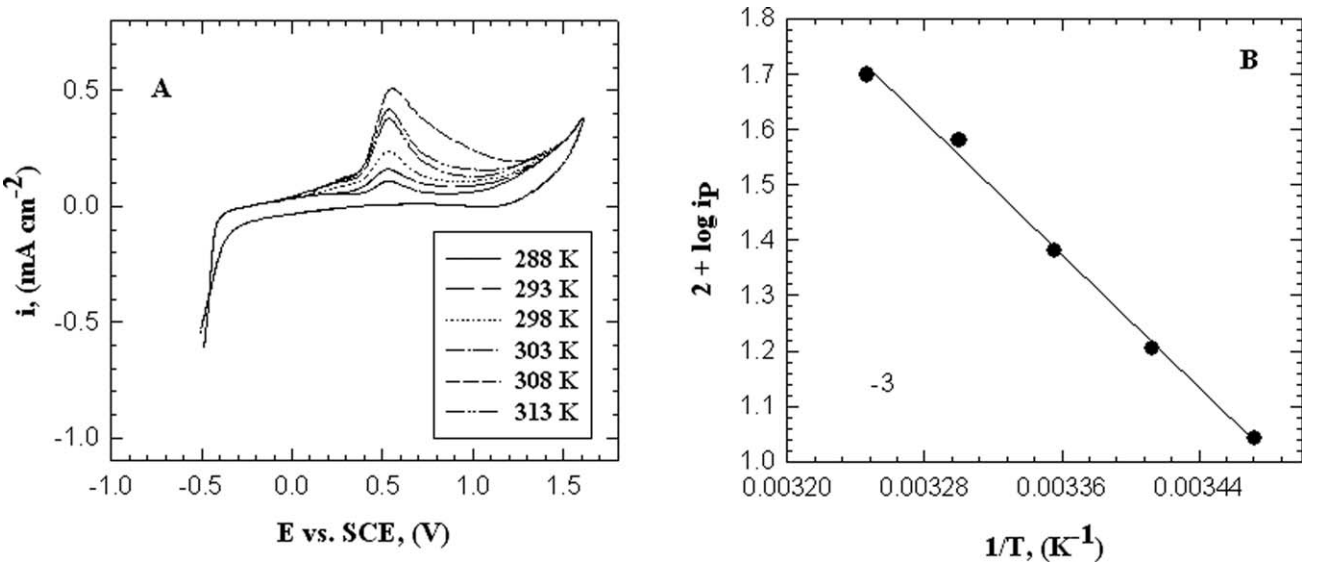

Figure 7 A: Cyclic voltammetry curves for the effect of temperature on the electropolymerization of a binary mixture of *o*PD and 2ABT from solution containing 0.5 *M* HCl, 0.05 *M* (1 : 1 molar ratio) monomer and 1 *M* Na_2SO_4 at 303 K with scan rate of 25 mVs^{-1}. B: Arrhenius plot of the electropolymerization of the mixture of *o*PD and 2ABT.

- The second and third decomposition stages include the loss of the dopant species, HCl, and SO_3.[12–16]
- The fourth decomposition stage, in the range of 350 up to 600°C at which the copolymer sample began to decompose.
- The last stage, above 600°C, the weight loss was found to be 44.95%, which is attributed to the remaining benzenoid and thiazole moieties.

The IR spectrum of the prepared copolymer P(*o*PD-co-2ABT) in comparison with those of the two homopolymers P(*o*PD) and P(2ABT) are shown in Figure 9. From the Figure, it is clear that the medium absorption band appearing at 618 cm^{-1}, which may be attribute to C—S symmetrical stretching deformation in case of the P(2ABT), appears as a weak absorption band in case of copolymer at 600 cm^{-1}. The weak absorption band appearing at 691 cm^{-1}, which may be attributed to the wagging deformation of NH_2 in case of the P(*o*PD), appears as a medium absorption band in case of the P(2ABT) at 665 cm^{-1} and appear at 670 cm^{-1} as a weak band in case of the copolymer. The two weak absorption bands appearing at 721 cm^{-1} and 760 cm^{-1}, which may be attributed to the CH stretching vibration of benzene ring in case of the P(2ABT), appears as a medium and strong absorption bands in case of P(*o*PD) at 726 and 752 cm^{-1}, respectively, appears at 757 cm^{-1} as a weak band in case of the copolymer. The CH out-of-plane deformation appear as weak bands at 800, 841, and 887 cm^{-1} in case of P(*o*PD), at 815, 853, and 884.4 cm^{-1} in case of P(2ABT) and at 825 and 886 cm^{-1} in case of the copolymer. The weak bands appearing at 1130, 1143, and 1115 cm^{-1} in case of P(*o*PD), P(2ABT), and copolymer, respectively, could be attributed to the doping with SO_4^{-2} anions, while the doping with Cl^- anion is observed as a weak bands at 1169, 1171, and 1148 cm^{-1} in case of P(*o*PD), P(2ABT), and copolymer, respectively. Accordingly, both SO_4^{2-} and Cl^- anions are doped in the polymeric chain,[26,27] but no evidence for the formation of new bonds between the polymer chain and the doped anions was observed which means that the anions doped in the polymeric chains exist in the ionic form[28] as shown in Scheme 1. The medium band at 1634 cm^{-1} in case of P(2ABT) which could be attributed to the C=N stretching vibration of quinoide structure appears as a weak band at 1565 cm^{-1} in case of the copolymer. The other IR absorption bands and their assignments are tabulated in Table V.

TABLE II
Data of E_a Under Changing Scan Rate

Scan rate ($mV\ s^{-1}$)	−Slope	E_a ($kJ\ mol^{-1}$)	r^2
20	3.08	58.97	0.979
25	3.00	57.44	0.995
30	3.07	59.16	0.989

r^2 is the correlation coefficient.

The UV-visible spectra of P(*o*PD), P(2ABT), and there copolymer P(*o*PD-co-2ABT) are represented in Figure 10. The spectra show the following absorption bands:

1. Three absorption bands appear at λ_{max} = 216, 233, and 268 nm, which may be attributed to

TABLE III
Elemental Analysis Data of the Prepared Homo- and Copolymers

		Elemental analysis				
		C (%)	H (%)	N (%)	Cl (%)	S (%)
No	Structure of polymer	Cal/found	Cal/found	Cal/found	Cal/found	Cal/found
1	P(*o*PD)	43.68	5.56	16.90	14.30	3.20
		43.17	5.78	15.20	13.80	3.00
3	P(2ABT)	34.38	3.52	10.00	20.30	15.70
		35.10	4.81	9.70	20.30	16.00
4	P(*o*PD-co-2ABT)	60.10	2.61	13.50	18.80	7.00
		59.53	2.89	12.80	18.40	6.90

π–π^* transition (E_2 – band) of the benzene ring and the β–band π–π^* transition (A_{1g}–B_{2u}), in case of copolymer appears as two absorption bands at 269 nm and 280 nm in case of P(*o*PD) and at 207 nm and 315 nm in case of P(2ABT).

2. A shoulder appears at λ_{max} = 438 nm, which could be attributed the high conjugation of the aromatic polymeric chain, in case of the copolymer, appears as a shoulder at 468 nm in case of P(2ABT) and as an adsorption band at 482 nm in case of P(*o*PD).

The specific conductivity of the copolymer was measured on a compressed pellet made by compressing the powder copolymer. The conductivity was measured with direct current from 5 to 25V—in this range the sample showed Ohmic behavior—and found to be 3.1×10^{-8} S cm^{-1}.

The obtained copolymer samples have low solubility in most polar and nonpolar solvents, and it is difficult to determine its ^{1}H-NMR signal (in both chloroform and DMSO) and its GPC data as molecular weight (in THF medium). Solubility data are listed in Table VI.

To confirm structure of the copolymer tools like IR, UV-vis, TGA,...,etc., are used else where.[29,30] Also the monomer reactivity ratio must be used.

Copolymer structure and the mechanism

The monomer reactivity ratios of the copolymerization system (r_1 and r_2) involving *o*-phenylenediamine (*o*PD) and 2-aminobenzothiazole (2ABT) were determined on the basis of comonomer composition–copolymer composition relationship. The monomer reactivity ratios were calculated according to Fineman-Röss method[31] using S-content as a quantitative analytical tool.

The oxidative electrocopolymerization was carried out as described previously under point 2.3 but with different molar ratios of the two monomers.

When two monomers such as *o*PD (M_1) and 2ABT (M_2) are copolymerized, there are two kinds of free radicals which form the growing chains. These two

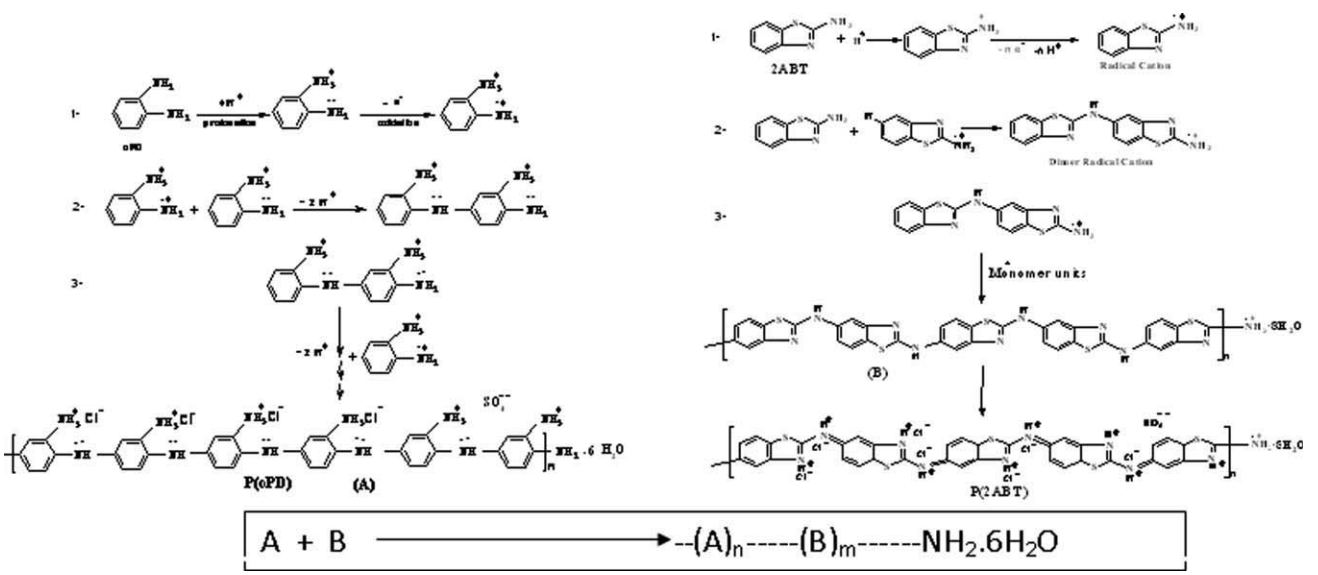

Scheme 1 Propagation and formation of the block copolymer.

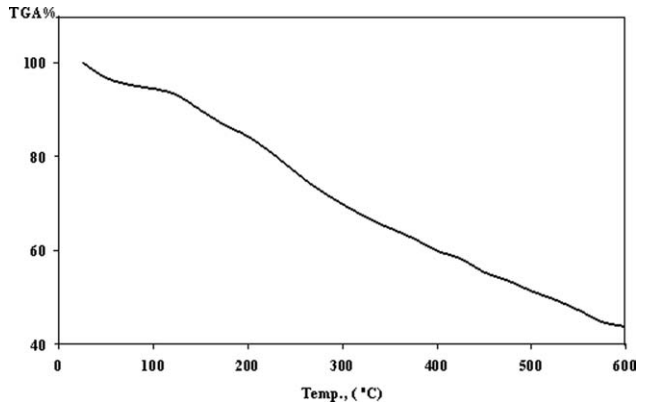

Figure 8 TGA curve for the prepared P(*o*PD-co-2ABT) copolymer.

kinds of chain radicals are designated as $M_1\bullet$ and $M_2\bullet$. The propagation reactions include four distinctly different equation,[32,33]

$$-M_{1\bullet} + M_1 \xrightarrow{k_{11}} -M_1M_{1\bullet} \quad (1)$$

$$-M_{1\bullet} + M_2 \xrightarrow{k_{12}} -M_1M_{2\bullet} \quad (2)$$

$$-M_{2\bullet} + M_1 \xrightarrow{k_{21}} -M_2M_{1\bullet} \quad (3)$$

$$-M_{2\bullet} + M_2 \xrightarrow{k_{22}} -M_2M_{2\bullet} \quad (4)$$

By derivation,[32,33] the copolymer composition equation may be write as:

$$F_1 = \frac{r_1 f_1^2 + f_1 f_2}{r_1 f_1^2 + 2 f_1 f_2 + r_2 f_2^2}$$

This equation relates the composition of the copolymer formed to the instantaneous composition of the feedstock and to the reactivity ratios r_1 and r_2 which characterize the specific system

The reactivity ratios r_1 and r_2 can be computed by plotting the data according to the Fineman-Röss method.[31] The composition of the copolymer was quantitatively determined by S-content in the copolymer samples, and the monomer reactivity ratios r_1 and r_2 of this copolymer was calculated from Fineman–Röss equation and represented in Figure 11.

TABLE IV
TGA Data of Prepared P(*o*PD-o-2ABT)

Temperature range (°C)	Weight loss (%)		The removed molecules
	Calculated	Found	
Room–108	5.20	5.17	$6H_2O$
108–222	14.80	15.32	$2\ SO_3 + 3\ HCl$
222–350	15.52	14.95	8 HCl
350–600	22.64	21.42	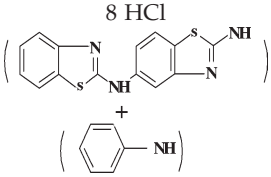
Above 600	–	41.75	Remaining units and metallic residues

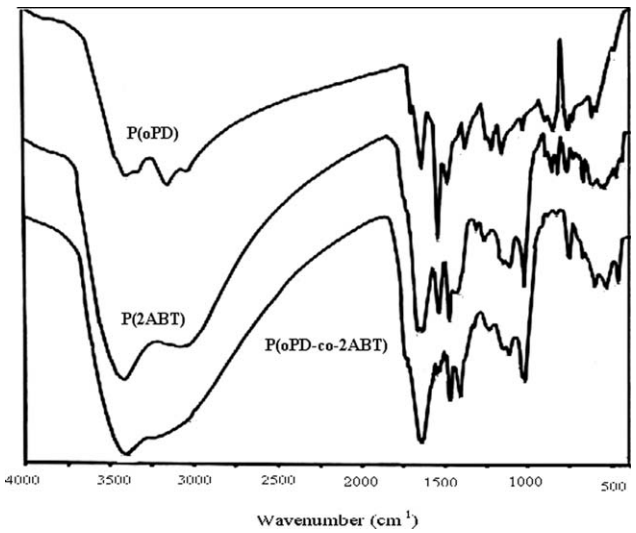

Figure 9 The IR-Spectra of P(*o*PD), P(2ABT), and P(*o*PD-co-2ABT).

$$F/f(f-1) = r_1(F^2/f) - r_2$$

where,

- $F = M_1/M_2$ (molar ratio for monomer feed composition)
- $f = m_1/m_2$ (molar ratio for copolymer composition)

The slope is equal to r_1 and the intercept is equal to $-r_2$. From the Figure, it was found that $r_1 = 1.62$ and $r_2 = 0.13$. From the data, the value of r_1 is more than one and r_2 is less than one. In this case, the propagation reaction Type 11 and 21 will be preferred than the Type 12 and 22, hence the probability of M_1 (*o*PD) entering into the copolymer chain is higher as compared to M_2 (2ABT), therefore the formed copolymer will be richer in M_1.

The copolymer composition data for the investigated system were calculated and the relation between the mole fraction of M_1 in the formed copolymer (n_1) and the mole fraction of M_1 in the monomer feed (N_1) and are plotted in Figure 12. The diagonal line represents the case that both monomers have identical reactivity. The values of n_1 for the copolymers are above the diagonal line indicating that the copolymers consist of a higher fraction of *o*PD units than that of 2ABT units and that the *o*PD is much more reactive than 2ABT. However, the product of $r_1 r_2 = 0.21$ ($<<1$), indicating that the copolymerization show an alternating tendency.[34]

From the above data, it is clear that the copolymer structure is a block copolymer structure with

TABLE V
Infrared Absorption Bands of the IR Spectrum of P(PD), P(2ABT), and P(*o*PD-co-2ABT) Samples

Wavenumber (cm^{-1}) Names			
P(*o*PD)	P(2ABT)	Copolymer	Assignments
472.5^{w}	409.4^{w}	466^{m}	CH wagging deformation
	428.6^{w}		of 1,2 –disubstituted
	464.4^{w}		benzene ring
510^{vw}	518.8^{w}	537^{w}	Out-of-plane deformation
584^{m}	537.8^{w}		of ring
–	618^{w}	600^{w}	C—S symmetrical vibration
691^{w}	665.6^{m}	670^{w}	NH_2 wagging deformation
726.7^{m}	721.2^{w}	757^{w}	CH stretching vibration of
752^{s}	760^{w}		benzene ring
800^{w}	815^{w}	825^{w}	CH out-of-plane deformation
841.1^{w}	853^{w}	886^{w}	
887^{ws}	884.5^{w}		
1020^{m}	1020^{s}	1021.5^{s}	CH in-plane deformation
1050^{w}	–	–	NH_2 twist deformation
1120^{vw}	–	–	CH stretching vibration
1145^{vw}			
1205^{s}			
1130^{w}	1143^{w}	1115^{w}	SO_4^{-2} incorporation
1169^{w}	1171^{w}	1148^{w}	Cl^{-1} incorporation
1250^{w}	1255^{w}	1231.7^{w}	C—NH_2 stretching vibration
1365^{s}	–	–	C—C stretching vibration
1400^{vw}			
1474^{s}			
1529^{s}			
–	1634^{m}	1565^{w}	C=N stretching vibration
1624^{s}	1652^{m}	1640^{s}	NH_2 scissoring vibration
1685^{vw}			
3008^{vw}	3066^{b}	3045^{b}	CH stretching vibration
3028^{w}			
3139^{b}	–	–	NH_2 symmetric vibration
3200^{b}	–	–	NH_2 asymmetric stretching
			vibration of aromatic amine
3385^{b}	3402^{b}	3391^{b}	NH_2 asymmetric stretching
			vibration of aromatic amine
			or OH strong hydrogen
			bonded group in H_2O
			molecules of hydration
			in polymer

s, strong; w, weak; b, broad; m, medium; vw, very weak.

alternative tendency, the supposed mechanism and the rate equations are applicable to copolymerization reaction between *o*PD and 2ABT. The mechanism is shown in Scheme 1.

Surface morphology

In most conditions, a homogeneous, smooth, and well-adhering P(*o*PD), P(2ABT), and P(*o*PD-co-2ABT) films were electrodeposited on platinum electrodes surface.

The X-ray diffraction pattern shows that the prepared P(*o*PD) is amorphous material,[35] while P(2ABT) is crystalline, where there are two peaks at 2θ angle equal to 18.88 and 21.26, and P(*o*PD-co-2ABT) is crystalline where there is a peak at 2θ angle equal to 21.18. The surface morphology of the polymer obtained at the optimum conditions was examined by scanning electron microscopy. [c.f. Fig. 13(A)]

The SEM micrograph shows a smooth surface feature with uniform thickness and has amorphous nature for P(*o*PD),[35] a smooth surface feature has

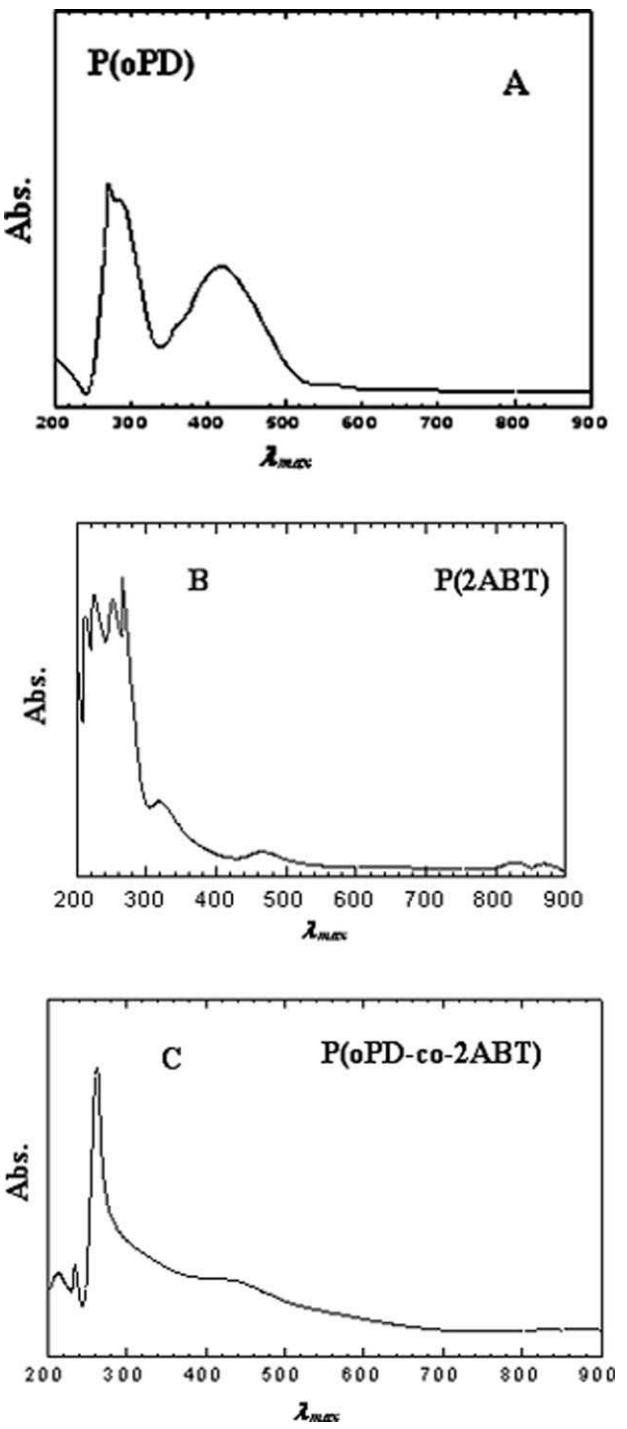

Figure 10 UV-vis absorption spectra of; A: P(*o*PD), B: P(2ABT), and C: P(*o*PD-co-2ABT).

TABLE VI
Solubility Data for the Copolymer Samples

Solvents	P(*o*PD)	Copolymer composition (*o*PD : 2ABT) molar ratio					P(2ABT)
		90 : 10	70 : 30	50 : 50	30 : 70	10 : 90	
Acetone	○	○	○	○	◊	◊	●
Methanol	○	○	○	○	◊	◊	●
Ethanol	○	○	○	○	◊	◊	●
DMF	●	●	●	●	●	●	●
DMSO	●	◊	◊	◊	◊	◊	●

●, soluble; ◊, slightly soluble; ○, insoluble.

tubular or fibrillar elongated crystals for P(2ABT) and an amorphous feature with (small portion of crystallinity tubular or fibrillar elongated crystals) for P(*o*PD-co-2ABT) [c.f., Fig. 13(B)].

CONCLUSIONS

In conclusion, the above data reveals the following:

The initial rate of electropolymerization reaction of a binary mixture of *o*PD and 2ABT (1 : 1 *M* ratio) on platinum surface is relatively low. The fraction of the dissolved product in solution near the electrode surface may be strongly dependent on temperature, monomer, and HCl concentrations.

The orders of the electrocopolymerization reaction are 1.09, 2.08, and 0.84 with respect to HCl, monomer, and electrolyte concentration, respectively.

The apparent activation energy was calculated from Arrhenius equation and it is found to be 57.44 kJ mol^{-1}, this value is approximately the same at different scan rates.

The prepared P(*o*PD-co-2ABT) copolymer has a morphology in between the two separate homopolymers, which is amorphous feature with tubular or fibrillar elongated crystals and well adhered on platinum electrode surface.

From cyclic voltammetry studies, it is clear that the cyclic voltammogram consists of one irreversible peak at +532 mV vs SCE, which lies in between the two homopolymer oxidation potentials.

The electrodeposition of the copolymer film on platinum electrode may be described partially by a diffusion-controlled process.

The monomer reactivity ratios are found to be $r_1 = 1.62$ and $r_2 = 0.13$, and the copolymer structure is a block structure containing more rich in *o*PD units.

The proposed structure and the derived rate equation are applicable for the copolymerization reaction

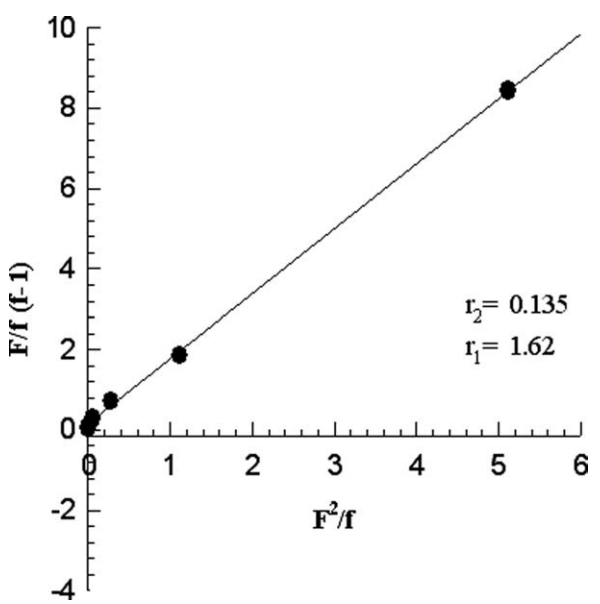

Figure 11 Fineman-Röss plot for the determination of monomer reactivity ratio of *o*PD (M_1) in HCl solution copolymerized by electrochemical method on Pt-electrode.

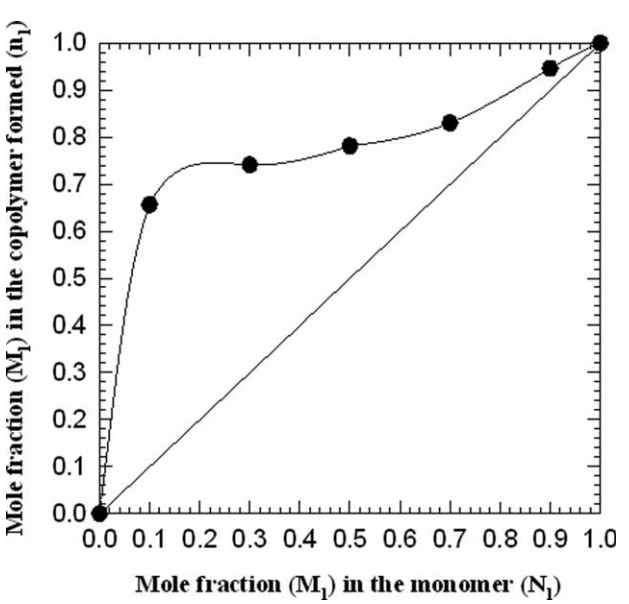

Figure 12 Composition curve for the electropolymerization between *o*PD (M_1) and 2ABT (M_2) from aqueous solution on Pt-electrode.

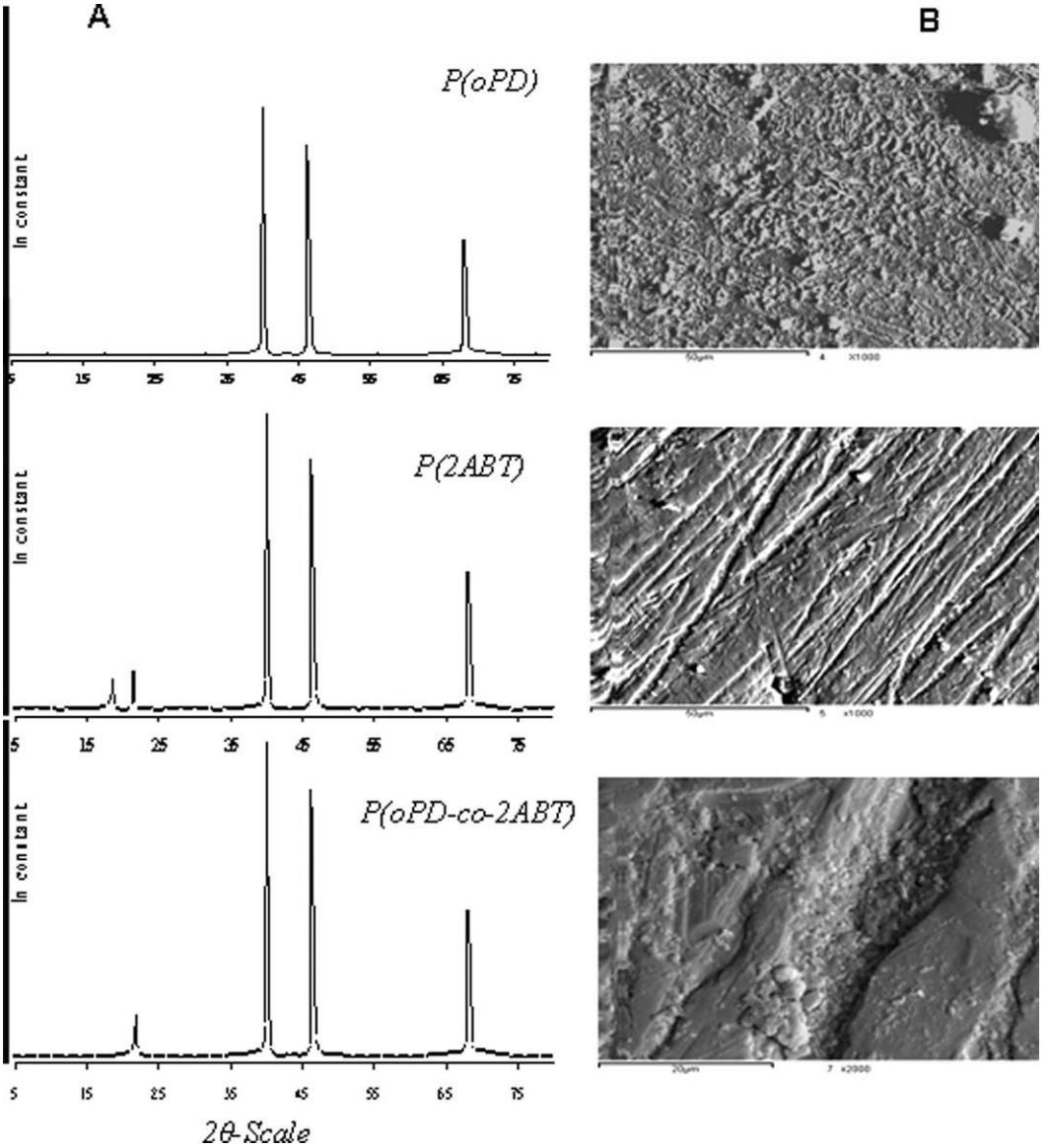

Figure 13 (A) X-ray diffraction pattern of P(*o*PD), P(2ABT), and P(*o*PD-co-2ABT). (B) The picture of SEM of P(*o*PD), P(2ABT), and P(*o*PD-co-2ABT).

below 0.5 *M* HCl, 0.05 *M* comonomer (1 : 1) molar ratio, 0.1 *M* Na_2SO_4, 303 K, and scan rate 25 mVs^{-1}.

The specific conductivity of the copolymer was found to be 3.1×10^{-8} S cm^{-1}.

References

1. Li, X. G.; Huang, M. R.; Duan, W.; Yang, Y. L. Chem Rev 2002, 102, 2002.
2. Nakabayashi, Y.; Yoshikawa, H. Anal Sci 2000, 16, 609.
3. Reemtsma, T.; Fiehn, O.; Kalnowski, G.; Jekel, M. Environ Sci 1995, 29, 478.
4. Bujdakova, H.; Kralova, K.; Sidoova, E. Pharmazia 1994, 49, 375.
5. Meding, B.; Toren, K.; Karlberg, A. T.; Hgberg, S.; Wass, K. Am J Ind Med 1993, 23, 721.
6. Ibrahim, A. M. A.; Etaiw, S. E. H. Polyhedron 1997, 16, 1585.
7. Sayyah, S. M.; El-Deeb, M. M.; Abdel-Rehim, S. S. Int J Polym Mater 2004, 53, 941.
8. Sayyah, S. M.; El-Deeb, M. M. J Appl Polym Sci 2007, 103, 4047.
9. Sayyah, S. M.; Abd El-Rehim, S. S.; El-Deeb, M. M. J Appl Polym Sci 2003, 90, 1783.
10. Sayyah, S. M.; Abd El-Rehim, S. S.; El-Deeb, M. M. J Appl Polym Sci 2004, 94, 941.
11. Sayyah, S. M.; Kamal, S. M.; Abd El-Rehim, S. S.; Ibrahim, M. A. Int J Polym Mater 2006, 55, 339.
12. Sayyah, S. M.; Azooz, R. E.; El-Rabiay, M. M.; Abd El- Rehim, S. S. Int J Polym Mater 2006, 55, 37.
13. Sayyah, S. M.; Kamal, S. M.; Abd El-Rehim, S. S. Int J Polym Mater 2006, 55, 79.
14. Sayyah, S. M.; El-Rabiay, M. M.; Abd El-Rehim, S. S.; Azooz, R. E. J Appl Polym Sci 2006, 99, 3093.
15. Sayyah, S. M.; Kamal, S. M.; Abd El-Rehim, S. S. Int J Polym Mater Sci 2007, 56, 663.
16. Sayyah, S. M.; Abd El-Rehim, S. S.; El-Deeb, M. M.; Kamal, S. M.; Azooz, R. E. J Appl Polym Sci 2010, 117, 943

17. Randless, J. P. Trans Faraday Soc 1948, 44, 327.
18. Sevick, A. Collect Czech Chem Commun 1948, 13, 349.
19. Mazloum-Ardakani, M.; Sadeghiane, A.; Moosavizadeh, S.; Karimi, M. A.; Mashhadizadeh, M. H. Anal Bioanal Electrochem 2009, 1, 224.
20. Nicholson, R. S. Anal Chem 1965, 37, 1351.
21. Rieger, P. H. Electrochemistry; Wiley: New York, 1985.
22. Ureta-Zanartu, M. S.; Butos, P.; Berríos, C.; Diez, M. C.; Mora, M. L.; Gutiérrez, C. Electrochim Acta 2002, 47, 2399.
23. Mu, S.; Chen, C.; Wang, J. Synth Met 1997, 88, 249.
24. Kitane, A.; Yano, J.; Kuani, A.; Sasaki, K. J Electroanal Chem 1987, 221, 69.
25. Becerik, I.; Ficiciogluand, F.; Kadirgan, F. T. J Chem 1999, 23, 353.
26. Buzarovska, A.; Arsovo, I.; Arsov, L. J. Serb Chem Soc 2001, 66, 27.
27. Nakanishi, K.; Solomon, P. H. Infrared Absorption Spectroscopy; Holden–Day: San Francisco, 1977.
28. Athawale, A. A.; Deore, B.; Vedpathak, M.; Kulkarni, S. K. J Appl Polym Sci 1999, 74, 1286.
29. Raghu, A. V.; Gadaginamath, G. S.; Jawalkar, S. S.; Halligudi, S. B.; Aminabhavi, T. M. J Polym Sci A Polym Chem 2006, 44, 6032.
30. Raghu, A. V.; Gadaginamath, G. S.; Mathew, N.; Halligudi, S. B.; Aminabhavi, T. M. J Appl Polym Sci 2007, 106, 299.
31. Finman, M.; Ross, S. D. J Polym Sci 1950, 5, 250.
32. Mayo, F. R.; Lewis, F. M. J Am Chem Soc 1944, 66, 1594.
33. Gowaiker, V. R.; Viswanathan, N. V.; Sreedhar, J. Polymer Science; Halsted Press: New York, 1986; p 193.
34. Wei, J.; Zhu, Z.; Huang, J. J Appl Polym Sci 2004, 94, 2376.
35. Sayyah, S. M.; El-Deeb, M. M.; Kamal, S. M.; Azooz, R. E. J Appl Polym Sci 2009, 112, 3695.